

Photosensitization of thin SnO₂ nanocrystalline semiconductor film electrodes with electron donor–acceptor metallodiporphyrin dyad

Miguel Gervaldo, Luis Otero, M. Elisa Milanesio, Edgardo N. Durantini, Juana. J. Silber, Leonides E. Sereno *

Departamento de Química, Universidad Nacional de Río Cuarto, Agencia Postal 3, 5800 Río Cuarto, Argentina

Received 19 July 2004; accepted 19 November 2004
Available online 13 December 2004

Abstract

A electron donor–acceptor porphyrin dyad ($P_{Zn}-P$) was synthesized by linking an electron acceptor porphyrin; 5,15-bis(4-carboxyphenyl)-10,20-bis(4-nitrophenyl) porphyrin (P) and an electron donor porphyrin; Zn(II) 5-(4-aminophenyl)-10,15,20-tris(4-methoxyphenyl) porphyrin (P_{Zn}) by amide bond. $P_{Zn}-P$ dyad – thin SnO₂ nanocrystalline semiconductor film electrodes show higher spectral sensitized photocurrent quantum yield compared to the electrodes sensitized with either P_{Zn} or P monomers. Fluorescence analysis of dyad and the P moiety adsorbed on both, SnO₂ semiconductor and SiO₂ insulator, shows that the charge injection yields (Φ_{inj}) from the excited dyes to the SnO₂ are similar in both cases. Thus photocurrent enhancement is interpreted in terms of intramolecular electron transfer and preferential spatial orientation of the dyad on the SnO₂ surface that preclude back electron transfer.

© 2004 Elsevier B.V. All rights reserved.

1. Introduction

The spectral sensitization of wide band gap metal oxide semiconductors with organics dyes is of great interest in the search of efficient energy conversion devices [1–4]. A considerable number of organic structures has been designed, synthesized and studied with this purpose, and many researchers were inspired in this field by the natural photosynthetic apparatus [5–15]. Photo-initiated transmembrane electron transfer to yield long-lived charge-separated states is the basic energy conversion process of natural photosynthesis. In the protein environment of photosynthetic reaction centers the process is carried out by a series of short-range, fast,

and efficient electron-transfer steps, which move electrons and holes to opposite sides of the membrane [16,17]. One approach to mimic the photosynthetic energy conversion system in nature is the use of complex synthetic molecular arrays containing chromophores, electron donors and electron acceptors linked by covalent and non-covalent bonds [17–25]. The energy stored in these systems as a photoinduced intramolecular charge separation state can be converted in electric work through an external circuit in a suitable photoelectrochemical cell. On the other hand, many studies on the development of optoelectronic and energy conversion devices incorporate several metallized and unmetallized tetrapyrrolic compounds, as light receptors and charge storage units [26–32].

It is interesting to remark the analogies between the natural photosynthesis and the dye-sensitized nanocrystalline semiconductor electrodes using electron

* Corresponding author. Tel.: +54 358 4676541; fax: +54 358 4676233.

E-mail address: lsereno@exa.unrc.edu.ar (L.E. Sereno).

donor–acceptor molecular assemblies [33]. In a porous film of nanometer-sized semiconductor particles, the effective surface area can be greatly enhanced, producing substantial light absorption [34–41] and charge separated states formation. Light harvesting and charge separation efficiencies in a range of porphyrin dyes adsorbed on nanostructured semiconductor oxides were found comparable to those in natural photosynthesis, with a very high (nearly 80%) incident-photon-to-current efficiency (IPCE) [5,6]. With such high efficiencies, the photosensitization of oxide semiconductors has become a practical mean for solar energy conversion. Using Ru(II) bipyridine complexes as photo-sensitizers, net power conversion efficiencies up to 10% have been reported in diffuse daylight on nanoporous TiO₂ electrodes [1,2,42,43].

Imahori et al. [44–46] reported the production of photocurrent output with very high quantum yield by using donor–acceptor linked molecules, composite molecular nanoclusters [47] and quaternary self-organization of donor–acceptor dye units [48]. Likewise, we recently synthesized a porphyrin–fullerene dyad molecule, which showed to be effective in the spectral sensitization of wide band gap SnO₂ nanostructured semiconductor electrode, producing anodic photocurrents under visible irradiation [49]. Regardless of the fact that the porphyrin fluorescence was strongly quenched by the C₆₀ moiety in the dyad, the photocurrent generation quantum yield was around twice in the dyad when it is compared with the same yield of the porphyrin moiety. A mechanism involving the formation of an intramolecular photoin-

duced charge transfer state was proposed in order to explain the observed photoeffect [49].

On the other hand, in a recent work, we used a porphyrin dyad molecule and its structural moieties in the spectral sensitization of wide band gap SnO₂ nanostructured semiconductor electrode [50,51]. SnO₂ film modified with porphyrin dyes exhibited photoresponse in the visible region, and nearly complete singlet–singlet energy transfer from Zn-porphyrin to free base moiety was observed in the dyad in the adsorbed state. Consequently, a suitable “antenna” effect was obtained using the dyad molecule. However, the photocurrent efficiency in the dyad was lower than the one produced by the free base moiety. This fact was explained considering that the metallized porphyrin enhances the back electron transfer process, producing low photocurrent yield [52,53]. However, the lack of preferential orientation of the dyad over the SnO₂ surface (i.e., whether it is the free base moiety or the Zn-porphyrin moiety that gets attached to SnO₂ surface) also play a role in determining the photocurrent quantum yield of the dyad [51,54].

Thus, in order to improve the photocurrent quantum yield, we designed and synthesized [55] a novel porphyrin–porphyrin supramolecular arrangement with particular structural and electronics properties. The new asymmetric dyad **P_{Zn}–P** (Fig. 1) was designed in order to increase the intramolecular electron transfer capacity; one porphyrin moiety (**P_{Zn}**) bears electron-donating methoxy groups and a zinc ion, which help to stabilize

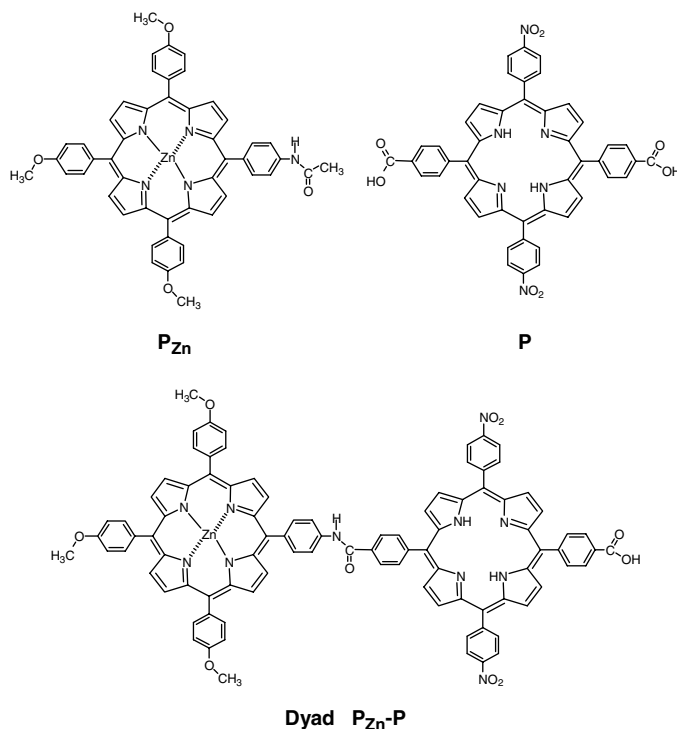


Fig. 1. Structures of the sensitizing dyes.

the radical cation; the second porphyrin moiety (**P**) features electron-withdrawing nitro substituent, which stabilize the porphyrin radical anion. It has been demonstrated that peripheral substitution in para-substituted tetraphenylporphyrin [$H_2(p-X)TPP$] [56] and metalloporphyrins [57–59] ($[M(p-X)TPP]$ where $M = Mn^{2+}, Fe^{2+}, Co^{2+}, Ni^{2+}, Cu^{2+}$ and Zn^{2+}) has a noticeable effect in modulating their electron donor/acceptor capabilities. Hammett linear correlations between electron donating or withdrawing ability of p-X substituents showed that the stronger effects are produced by $-OCH_3$ and $-NO_2$ groups, the same that were selected by us in the design of the $P_{Zn}-P$ dyad. In $P_{Zn}-P$ dyad the moieties are linked by amide bond, which allows electronic interaction between the π systems of the two chromophores [60,61].

On the other hand **P** moiety bears a remnant carboxylic acid group. This group was conveniently located in the electron-withdrawing porphyrin moiety in order to benefit the orientation of the $P_{Zn}-P$ dyad with respect to the basic semiconductor oxide electrode [62,63]. The preferential orientation is able to improve charge injection and to keep the photooxidized porphyrin moiety away from the photoinjected electrons. This fact could diminish back electron transfer process [2,11,55]. Through the combination of intramolecular and interfacial photoinduced charge injection processes is expected to increase the photocurrent quantum yield of the dye sensitized photovoltaic system [64,65].

2. Experimental

2.1. Synthesis of porphyrine dyes

The structures of the porphyrins used are shown in Fig. 1. 5,15-Bis(4-carboxymethylphenyl)-10,20-bis(4-nitrophenyl) porphyrin (**ester-P**) was synthesized from

the reaction of *meso*-(4-nitrophenyl) dipyrromethane with 4-carboxymethylbenzaldehyde in a MacDonald-type 2 + 2 condensation [66]. The hydrolysis in basic medium of **ester-P** yielded 5,15-bis(4-carboxyphenyl)-10,20-bis(4-nitrophenyl) porphyrin (**P**). 5-(4-Acetamidophenyl)-10,15,20-tris(4-methoxyphenyl) porphyrin (**amido-P**) was formed from the condensation of *meso*-(4-methoxyphenyl)dipyrromethane with a binary mixture of 4-methoxybenzaldehyde and 4-acetamidobenzaldehyde according to the procedure previously described [67]. Basic hydrolysis of **amido-P** produced 5-(4-amidophenyl)-10,15,20-tris(4-methoxyphenyl) porphyrin (**amino-P**). Treatment of **amido-P** and **amino-P** with Zn(II) acetate was used to obtain the corresponding Zn(II) metallo complexes. To synthesize the target dyad $P_{Zn}-P$, the carboxylic acid group of the porphyrin **P** was transformed to acid chloride using thionyl chloride in dry toluene and pyridine. The acid chloride was immediately used for coupling with Zn(II) 5-(4-aminophenyl)-10,15,20-tris(4-methoxyphenyl) porphyrin. The reaction mixture was allowed to react for 15 h at room temperature. The product was purified by flash chromatographic column. Spectroscopic data of the porphyrin derivatives have been previously reported [55].

2.2. Preparation of nanocrystalline films

The SnO_2 nanostructured film thin electrodes were prepared using a modification of the Kamat's procedure [38] by the method already described [12,49]. As base contact optically transparent electrodes of indium tin oxide (ITO, 100 Ω /square, Delta Technologies) were used. ITO/ SnO_2 electrodes were prepared by spin coating using a P6204-A model Specialty Coating System. The final films were annealed at 450 $^{\circ}C$ for 1 h. The SnO_2 films were analyzed by X-ray diffractometry (Siemens D5000, Cu $K\alpha$ radiation, XRD) in order to

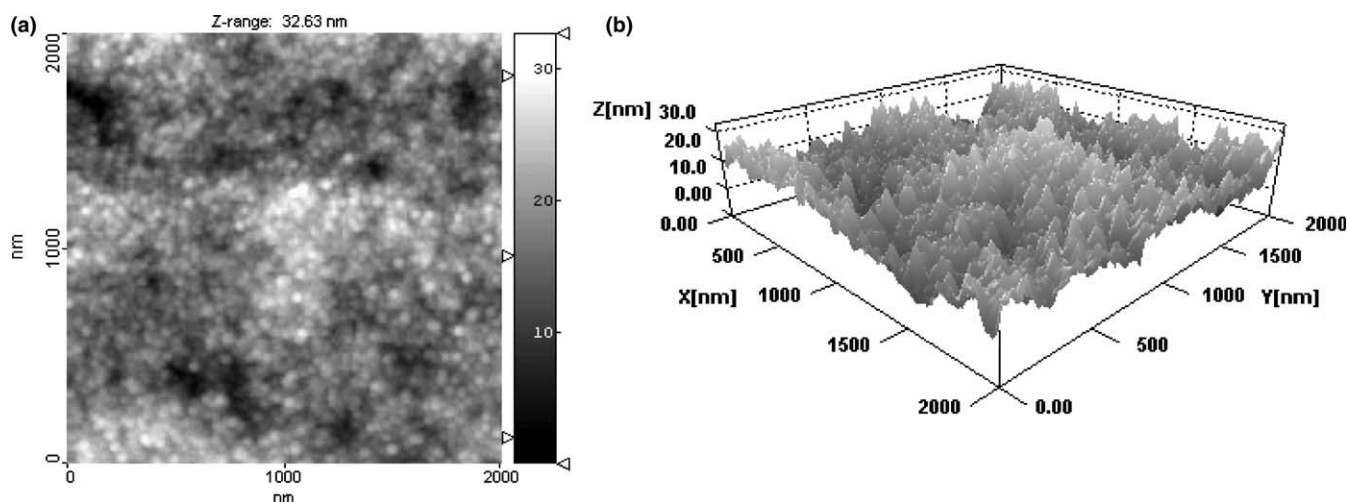


Fig. 2. Top view (a) and three-dimensional plot (b) AFM of the nanocrystalline SnO_2 film.

assess the crystallinity of the sample. The peaks in the X-ray diffraction pattern show lines which were in good agreement with the crystalline SnO₂ cassiterite standard [68,69]. To further investigate the morphological characteristics of the films, atomic force microscopy (Nanoscope III, AFM) has been used, operating in the tapping mode. Fig. 2(a) presents 2 μm × 2 μm top view of the films, meanwhile Fig. 2(b) shows a three-dimensional surface plot. The films consist of interconnected grain particles fused together to build up high mountains and deep valleys. The average grain diameter is about 15–20 nm and compares well the particle size of the initial colloid solution. This shows that no significant aggregation occurred during sintering of the film. The fractal analysis shows that the effective surface area is several times greater than the one of a flat non-fractal surface. Such surface not only permits the adsorption of a great number of dye molecules, but also creates a rough environment where multiple light reflections can occur, thus considerably increasing the amount of adsorbed photons. The nanoparticulate film obtained from colloidal suspension has a highly porous structure that permits a better wetting of the film by the electrolyte, which favors the interaction between the oxidized dye and the sacrificial donor.

SiO₂ nanostructured films were formed with the same procedure used for SnO₂ photoelectrodes, using a SiO₂ colloidal suspension in water (Ludox SM 30, Aldrich).

ITO/SnO₂ electrodes were modified with P_{Zn}-P dyad and the P_{Zn} and P porphyrin moieties (Fig. 1) soaking two hours ITO/SnO₂ films in a saturated n-hexane/dichloromethane (DCM Aldrich 99.8% grade) 80/20 solution of the corresponding dye. The electrodes were then washed with the same solvent, dried in nitrogen stream at room temperature and stored in vials. A copper wire was connected to the electrodes surface with an indium solder to achieve electric contact.

2.3. General

The voltammetric characterization of the redox process for the porphyrine dyes were acquired with a potentiostat-galvanostat Autolab (Electrochemical Instruments) using a Pt disc working electrode of 0.204 cm² and a Pt counter electrode in a conventional three compartment Pyrex cell. A freshly prepared Ag/AgCl quasireference electrode was used. This electrode was prepared by plating a thin layer of AgCl onto an Ag wire from a 1 × 10⁻³ M KCl solution. The working electrode was cleaned between each experiment by polishing with 0.3 μm alumina paste, followed by solvent rinses. Studies were carried out in N₂-degassed DCM with 0.1 M tetrabutylammonium hexafluorophosphate (TBAHFP, Aldrich) supporting electrolyte. The voltammograms were corrected for IR drop by positive feedback technique. After each voltammetric experiment,

ferrocene was added, and the potential axis was calibrated against the formal potential for ferrocenium/ferrocene redox couple ($E^0 = 0.46$ V vs SCE; 0.70 V vs NHE). All the potentials were referred to the normal hydrogen electrode (NHE) [51]. Redox potentials for the first anodic (E_{ox}) and cathodic (E_{red}) charge transfer of each molecule were calculated using the expression $(E_p \text{ forward} - E_p \text{ backward})/2$. The E_{ox} relative to the conventional scale (NHE) were converted to the absolute energy scale taken the energy of the electrons in NHE as -4.5 eV [70].

The oxidation potentials of the dye-excited state (E_{ox}^*) were estimated by subtracting the excitation energy from the redox potentials of the molecule in the ground state [70].

Absorption spectra were recorded on a Shimadzu UV-2401PC spectrophotometer. Fluorescence spectra were recorded on a Spex FluoroMax fluorimeter, provided of solid sample holder. The fluorescence quantum yields (ϕ_f) were obtained in degassed toluene solutions by comparison with that of tetra phenyl porphyrine (TPP, $\phi_f = 0.11$) used as fluorescence standard. Relative fluorescence intensities from photoelectrodes (I_f) were calculated from the area below the absorption corrected emission spectrum in air. Light harvesting efficiency (LHE) of the dye adsorbed over the photoelectrodes were obtained from $LHE = 1 - 10^{-A_\lambda}$, where A_λ is the monochromatic absorbance [41].

2.4. Photoelectrochemical measurements

Photoelectrochemical experiments were conducted in aqueous solutions (0.01 M) of hydroquinone (H₂Q, Aldrich, recrystallized from toluene), with phosphate buffer (pH = 5.2) prepared from 0.05 M NaH₂PO₄ (Anebra > 99%) and NaOH (Baker). These solutions were degassed by bubbling with Ar and maintained it in the top of the cell by continuous stream. The measurements were carried out under potential control in an already described quartz photoelectrochemical cell [49–51] equipped with Ag/AgCl as reference electrode, and Pt foil as the auxiliary electrode, using a computer controlled battery operated low noise potentiostat (Palm Sens). Action spectra were obtained by illumination of the photoelectrodes with monochromatic light obtained from a 75 W high-pressure Xe lamp (Photon Technology Instrument, PTI) and a computer controlled PTI high intensity grating monochromator. The steady-state photocurrents were obtained in front face configuration (illuminated area: 1 cm²). The incident light intensities at different wavelengths were measured with a Coherent Laser-Mate Q radiometer (sensitivity 1 μW).

2.5. Laser-flash photolysis experiments

Laser-flash photolysis set-up has been described elsewhere [49,71]. A Q-switched Nd:YAG laser (Spectron

SL400) was used as the excitation source operating at 532 nm (20 ns halfwidth) in order to excite the porphyrin compounds adsorbed over ITO/SnO₂ electrodes placed in the already described photoelectrochemical cell. Has been reported [53] that the electron injection kinetics into semiconductor are rather insensitive to experimental conditions. In contrast, the recombination kinetics between dye cation and photoinjected electrons are very strongly dependent upon experimental conditions, with variation in the recombination rate from picoseconds to milliseconds depending upon the excitation intensity, solvent/electrolyte composition and applied electrical bias [52,53,78]. To compare the recombination kinetics between the different sensitizer dyes, considerable care was taken to minimize such experimental variation. Applied potential on ITO/SnO₂/dye electrodes was kept under control in a three electrode configuration, in an Ar – degassed phosphate buffer solutions without sacrificial donor hydroquinone. The laser beam was abated by using neutral filters in order to avoid multiphotonic processes and/or photodegradation of the samples. The sample electrodes were matched in absorbance at 532 nm, the wavelength of the exciting laser pulse, within 10%. The output of the detector was coupled to a digital oscilloscope (Hewlett-Packard HP-54504A). About twenty shots were usually needed for averaging decay times, in order to get a good signal to noise ratio. The averaged signals were analyzed as multiple exponential decays by using a calculation software (Microcal Origin 4.1, Northampton, USA).

3. Results and discussion

3.1. Solution electrochemistry

The voltammetric characterization of the reduction and oxidation process of the dyes was carried out in order to know electron donor–acceptor capacity of each moiety, and the energy of the possible intramolecular charge separated state in **P_{Zn}–P** dyad. It has been reported [51,72] that the reduction and oxidation potentials of the dimeric porphyrins are similar to those of the combined individual monomeric units, hence the energy of the charge separated state in **P_{Zn}⁺–P[–]** has been estimated from the first oxidation potential (E_{ox}) of **P_{Zn}** and first reduction potential (E_{red}) of **ester–P**. The oxidation voltammogram of **P_{Zn}** is shown in Fig. 3. The first charge transfer process occurs in this metallized moiety at $E_{ox} = 0.92$ V, that is, at 0.48 V less anodic potential than that for **P** ($E_{ox} = 1.40$ V). This result is expected due to the presence of the central metal and the electron donor methoxy groups substituents in **P_{Zn}**. This is in agreement with previous results [56]. On the other hand, the free base porphyrin possesses two strong electron

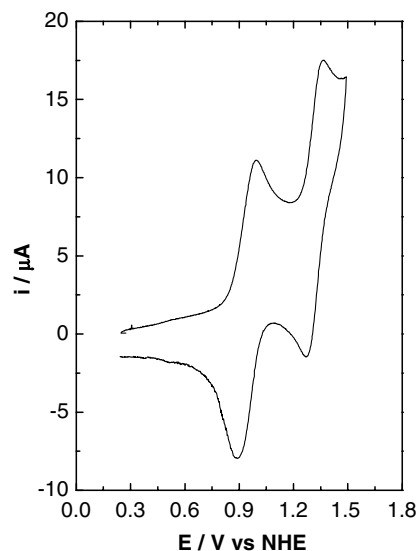


Fig. 3. Cyclic voltammogram at a platinum electrode ($A = 0.204$ cm²) of **P_{Zn}** 0.20 mM in DCM containing 0.1 M TBAHFP as supporting electrolyte, sweep rate = 0.100 V/s.

withdrawing nitro substituents, consequently, the reduction process (Fig. 1) for **P** ($E_{red} = -0.84$ V) is easier than the corresponding free base porphyrin without nitro groups. Taking into account all these values, it can be calculated that the **P_{Zn}⁺–P[–]** state in the dyad has an energy of 1.76 eV above its ground state.

3.2. Absorption and fluorescence spectra of dyes

The photochemistry of the monomers and dyad molecule was analyzed by steady-state absorption and emission spectroscopy. The absorption spectra of **P**, **P_{Zn}**, and **P_{Zn}–P** compounds are shown in Fig. 4, both in solution (toluene) and adsorbed over ITO/SnO₂ nanostructured films. As can be observed, the spectrum of the dyad (Fig. 4(c)) features the four Q-bands at λ_{max} 518, 554, 594 and 652 nm, whereas the Soret band appears at $\lambda_{max} = 424$ nm. The absorption spectrum is identical, within experimental error, with a linear combination of the spectra of the component chromophores (Fig. 4(a) and (b)) [67,72]. Thus, the absorption spectra are consistent with only a weak interaction between the moieties, and the two chromophores retain their individual identities in ground state [60]. On the other hand, porphyrin adsorption onto the semiconductor produces violet-green coloration of the film; the UV–Vis absorption spectra of the dye compounds on ITO/SnO₂/dye electrode show the Q and Soret bands with electronic transitions similar to those observed for monomeric absorption in solution. However, on the electrodes the bands are broader and are shifted in comparison with those in solution. This may be caused by the interaction of the porphyrins with the polar surface of the

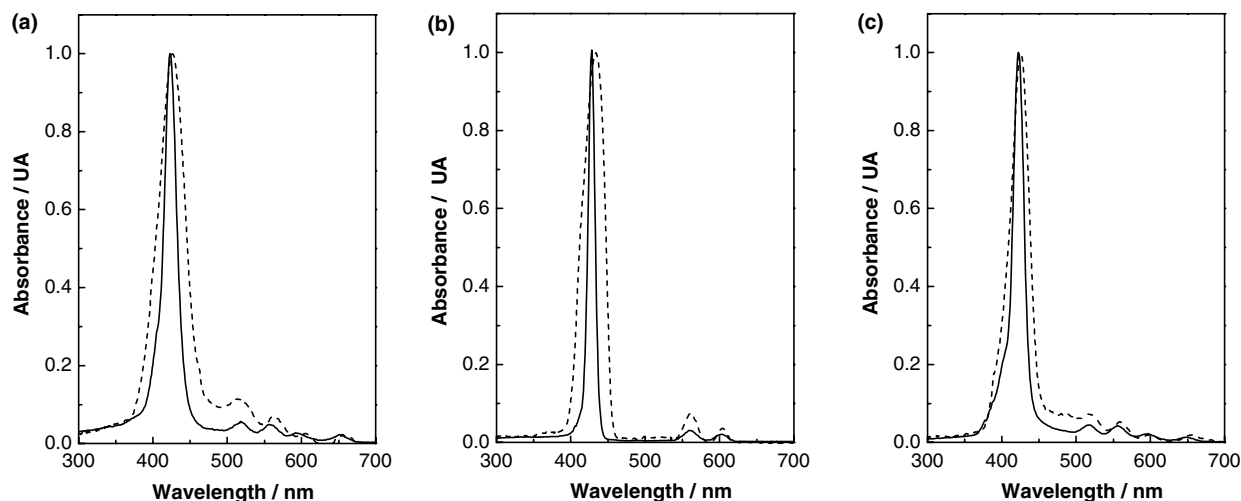


Fig. 4. Absorption spectra of porphyrins: in toluene solution (—) and in adsorbed state over ITO/SnO₂/electrodes (-----). (a) **P**; (b) **P_{Zn}** and (c) **P_{Zn}-P** dyad. Absorbance has been normalized to one at Soret band for comparison.

electrode, as well as the possible formation of porphyrin aggregates [51].

On the contrary, in the emission spectra this situation changes. Fig. 5(a) shows the absorption corrected fluorescence spectra of the monomers units and the dyad in toluene solution. The **P_{Zn}** has maxima at 604 and 652 nm, whereas **P** has two maxima at 653 and 719 nm. In this case, the emission spectra of the **P_{Zn}-P** dyad resemble that of the unmetallized porphyrin, with low emission from the **P_{Zn}** moiety, even though that both porphyrin species absorb at the excitation wavelength (550 nm). These results suggest singlet–singlet energy transfer in the **P_{Zn}-P** dyad from **P_{Zn}** moiety to the free base **P** [50,51,55,73]. Analyzing the possible photophysical mechanisms, the energies of the porphyrins first excited singlet states can be calculated from the average of the

frequencies of the longest wavelength absorption maxima and the shortest wavelength emission maxima. The obtained values for **P_{Zn}** and **P** first excited singlet states, 2.08 and 1.91 eV, respectively, show that there is a significant energy gap between both moieties in the dyad, thus, singlet–singlet energy transfer from the **P_{Zn}** to **P** is an energetically favorable process. The results show that the **P_{Zn}** moiety serves as a reasonable efficient antenna for **P** by transferring singlet excitation energy to it. However, it should be remarked that emissions from both porphyrin moieties are quenched in **P_{Zn}-P** dyad, relative to either monomer (fluorescence from the **P_{Zn}** and **P** are diminished with a quenching efficiency (η_q) of 0.62 and 0.35, respectively). Thus, the energy transfer is not complete, and the first excited singlet states of both porphyrins are quenched by another

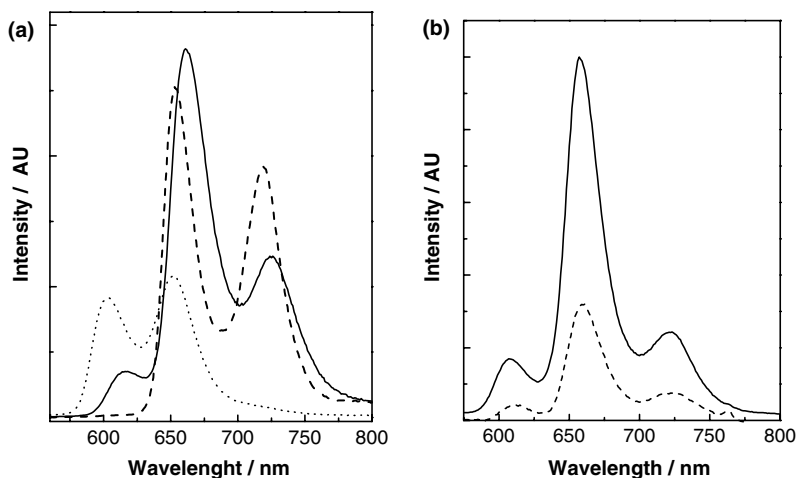


Fig. 5. (a) Corrected fluorescence emission spectrum in toluene solution of: **P** (-----); **P_{Zn}** (•••••) and **P_{Zn}-P** (—) dyad, $\lambda_{\text{ex}} = 550$ nm. (b) Fluorescence emission spectrum of **P_{Zn}-P** dyad adsorbed on SiO₂ (—) and SnO₂ (x2) (-----), $\lambda_{\text{ex}} = 420$ nm. All the emission spectra were corrected by the absorbance and instrumental response.

competitive process that could involve electron transfer from the \mathbf{P}_{Zn} to the \mathbf{P} moiety, producing the ion pair state, $\mathbf{P}_{Zn}^+-\mathbf{P}^{\cdot-}$ [55,60,61]. Since the electrochemical data shows that $\mathbf{P}_{Zn}^+-\mathbf{P}^{\cdot-}$ has a energy of 1.76 eV, this state lies at about 0.32 eV below \mathbf{P}_{Zn} first excited singlet state ($\mathbf{P}_{Zn}^1-\mathbf{P}$), making the intramolecular electron transfer quenching energetically feasible.

On the other hand, when the $\mathbf{P}_{Zn}-\mathbf{P}$ dyad is in adsorbed state (both, over SnO_2 and SiO_2 nanocrystalline films) the emission spectrum of an ITO/Oxide/ $\mathbf{P}_{Zn}-\mathbf{P}$ electrode also resembles that of the \mathbf{P} porphyrin, with no significant emission from the metallized moiety (Fig. 5(b)). This result suggests that singlet–singlet energy transfer from the \mathbf{P}_{Zn} to \mathbf{P} also occurs when the dye is adsorbed. However, the fluorescence intensity of the dyad adsorbed over SnO_2 film is much smaller than the same over the insulator SiO_2 (Fig. 5(b)). In other words, an additional quenching pathway is effective when the dyad is adsorbed on the semiconductor surface. This quenching can be interpreted in terms of electron transfer from the excited dye to the semiconductor [39]. In the present case, the energies of the excited dyad (in both possible singlet states, $\mathbf{P}_{Zn}^1-\mathbf{P}$ or $\mathbf{P}_{Zn}-\mathbf{P}^1$) are found to lie at higher values than the semiconductor conduction band edge [38] (vide infra). With all the described information an energy level diagram of the different states of $\mathbf{P}_{Zn}-\mathbf{P}$ dyad and the possible mechanism for the heterogeneous electron transfer in an ITO/ SnO_2 / $\mathbf{P}_{Zn}-\mathbf{P}$ electrode can be drawn as shown in Fig. 6.

After production of the excited state by photon absorption, several deactivation pathways are possible: radiative relaxation, thermal (non-radiative) relaxation, or interfacial charge injection. When the latter occurs

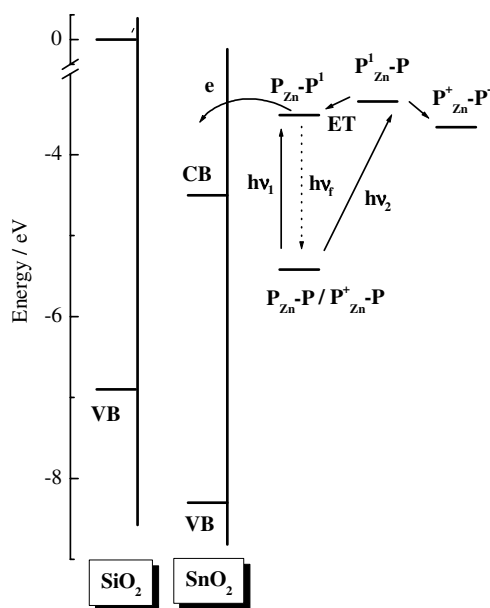


Fig. 6. Energy level diagram in absolute scale for the spectral sensitization of ITO/Oxide/ $\mathbf{P}_{Zn}-\mathbf{P}$ electrode. ET = energy transfer.

an external circuit could collect the injected electrons, producing observable photocurrent, although, the efficiency of charge harvesting is adversely influenced by charge recombination. On the other hand, when the dye is adsorbed on ITO/ SiO_2 (band gap = 6.9 eV) [74], the oxidation potential of the dye-excited state (E_{ox}^*) lies at much lower energy than the conduction band edge of the insulator. Consequently, electron transfer is not possible and the fluorescence is not affected by this additional mechanism [9]. On the contrary, for a dye adsorbed on ITO/ SnO_2 there is a driving force for photoinduced electron transfer from the dye to the semiconductor, defined as $\Delta E = -e(E_{ox}^* - E_{FB})$ [75], where E_{FB} is the potential of the semiconductor flat band (~ -0.02 V vs NHE) [38] and e is the electronic charge. Since electron transfer is in competition with radiative and non-radiative process, one can express the charge injection yield (Φ_{inj}) from the excited dye to the semiconductor as [9,76]:

$$\Phi_{inj} = \frac{k_{et}}{k_{et} + k_r + k_{nr}}, \quad (1)$$

where k_{et} is the heterogeneous electron transfer rate constant, k_r is the radiative deactivation rate constant and k_{nr} is the non-radiative deactivation rate constant. The electron transfer efficiency can be correlated with fluorescence quenching if the fluorescence intensity in absence of charge transfer ($I_{fl}(0)$) is written as:

$$I_{fl}(0) = A \cdot I_{exc} \frac{k_r}{k_r + k_{nr}}, \quad (2)$$

where A is an instrumental factor and I_{exc} is the excitation intensity. On the other hand, fluorescence intensity in the presence of electron transfer ($I_{fl}(e)$) can be written as:

$$I_{fl}(e) = A \cdot I_{exc} \frac{k_r}{k_{et} + k_r + k_{nr}}. \quad (3)$$

The reorganization of the Eqs. (2) and (3) gives Φ_{inj} in terms of normalized fluorescence intensities as follow:

$$\Phi_{inj} = \frac{I_{fl}(0) - I_{fl}(e)}{I_{fl}(0)}. \quad (4)$$

The relative fluorescence intensity (I_{fl}) obtained from the area below the corrected emission spectrum of photoelectrodes in air (Fig. 5(b)) allows to calculate the charge injection yield from dyes into the semiconductor nanoparticles (Eq. (4)). Φ_{inj} in this conditions was found to be 0.89 and 0.88 for $\mathbf{P}_{Zn}-\mathbf{P}$ dyad and \mathbf{P} porphyrin, respectively. Thus, the electron injection efficiency is similar for both compounds.

3.3. Photoelectrochemistry

The ITO/ SnO_2 /dye electrodes are photoelectrochemically active in the range between 300 and 700 nm. The

generated photocurrent is anodic, and negative open circuit photopotentials are observed upon excitation, indicating that the electrons flow from the solution to ITO base contact through the illuminated electrode. The photocurrent is reproducible under several (hundreds) repeated on–off illumination cycles. Contrarily, ITO/SiO₂/dye electrodes do not have photoresponse in the visible range, in agreement with the expected lack of charge injection into the insulator.

The action spectrums of ITO/SnO₂/dye electrodes (measured under 0.05 V positive bias vs. Ag/AgCl) closely match the absorption spectrum of the adsorbed organic molecules in all cases, as is shown in Fig. 7(a)–(c). The IPCE were evaluated from Eq. (5) [34,38,77].

$$\text{IPCE (\%)} = 100(i_{\text{sc}}1240)/(I_{\text{inc}}\lambda), \quad (5)$$

where i_{sc} is the short circuit photocurrent (A cm⁻²), I_{inc} is the incident light intensity (W cm⁻²), and λ is the excitation wavelength (nm). The close correspondence between the photocurrent action spectrum and the absorption spectrum of the electrodes confirms that photosensitization has successfully extended the photocurrent response of the electrodes into the visible region in all cases.

Maximum IPCE of ~3%, 2% and 10% were obtained at the Soret band of ITO/SnO₂/P, ITO/SnO₂/P_{Zn} and ITO/SnO₂/P_{Zn}-P, respectively. There are several reasons for this difference and may be linked to the factors that determine IPCE, namely, the LHE of the dye, the charge injection yield (Φ_{inj}) from the excited dye to the semiconductor, and the charge collection efficiency, η_c , of the system. The IPCE in terms of these parameters can be written [34,41] as:

$$\text{IPCE \%} = \text{LHE (\%)}\Phi_{\text{inj}}\eta_c. \quad (6)$$

Table 1 resume the results of IPCE, LHE and the product $\Phi_{\text{inj}}\eta_c$ for the three dyes at the Soret band. $\Phi_{\text{inj}}\eta_c$ allows to made a comparative analysis of photoelectric generation efficiency of the different dyes under similar experimental conditions.

As it can be observed P gives lower photocurrent efficiency than the metallized porphyrin, contrarily to the results that we obtained using structurally related molecules [51]. However, it must be noted that both porphyrins bear substituent groups that could affect the photoelectrochemical performance. In the case of the free base porphyrin P possess electron-withdrawing nitro substituents, which could be involved in a less effective heterogeneous electron injection into the semiconductor and/or faster back electron transfer. This deleterious process showed to be the main problem in achieving high IPCE values, producing low efficiency of photon to current efficiency [52,53]. Moreover, ana-

Table 1
Photoelectrochemical properties of dyes

Dye	SE ^a	$E_{\text{ox}}^{*,b}$	IPCE % ^c	LHE %	$\Phi_{\text{inj}} \times \eta_c$	$k_{\text{b}} \times 10^6 \text{ s}^{-1d}$
P	1.91	(-0.51)*	3	43	0.07	4.15 (79) 0.11 (21)
P _{Zn}	2.08	-1.16	2	14	0.14	2.7 (77) 0.09 (23)
P _{Zn} -P	–	–	10	38	0.26	2.37 (73) 0.10 (29)

^a Energy of the first excited singlet state (eV).

^b Oxidation potential of excited dyes (V vs NHE).

^c Maximum IPCE at Soret bands under bias voltage = 0.05 V.

^d Back electron transfer kinetic fitted by bi-exponential function, in parenthesis relative amplitudes.

* Taken from oxidation potential of ester-P.

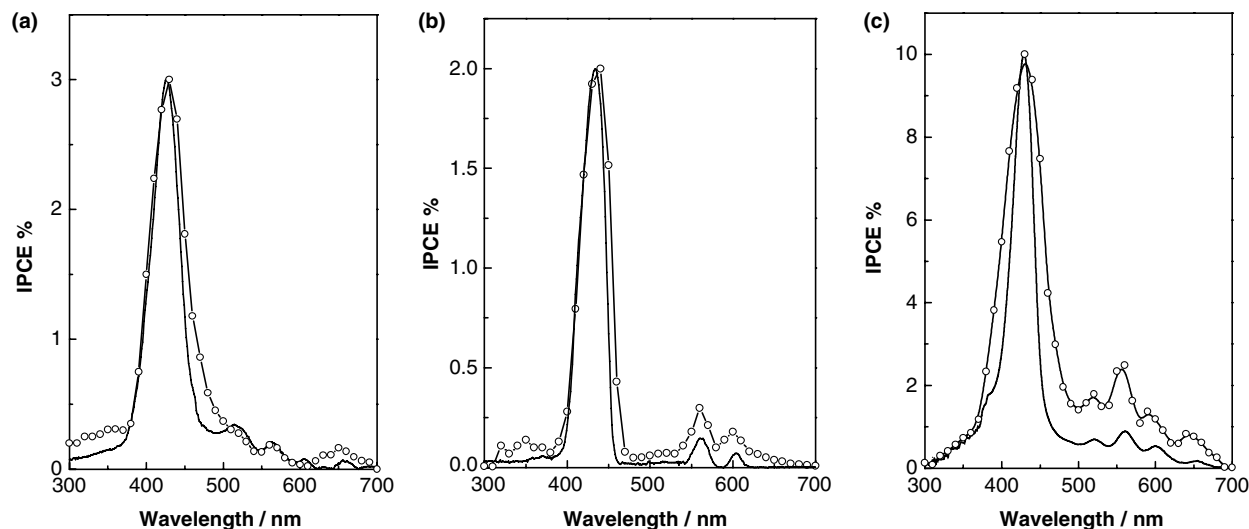


Fig. 7. Absorption spectra (—) and photocurrent action spectra, IPCE (-O-) of ITO/SnO₂/dye electrodes modified with (a) P; (b) P_{Zn}; and (c) P_{Zn}-P dyad.

lyzing the Φ_{inj} we found it to be large (0.88) and comparable to the same of $P_{Zn}-P$ dyad, which produces higher photocurrent quantum yield. Thus, low charge collection efficiency η_c of the ITO/SnO₂/P system could be the limiting factor through back electron transfer (i.e. the charge recombination between the photoinjected electron and the porphyrin cation). It has been showed by Tachibana and coworkers [53] that the electron injection kinetics from porphyrin and ruthenium complex sensitizers into TiO₂ conduction band are indistinguishable, meanwhile the recombination kinetics between the dye cations and electrons injected into the oxide film are strongly dependent upon experimental conditions, with variations from picoseconds to milliseconds in the recombination rates. It should be noted that $P_{Zn}-P$ dyad bears the remnant carboxylic acid group on the P moiety, which is located in the electron-withdrawing porphyrin moiety in order to benefit the orientation of the $P_{Zn}-P$ dyad on the semiconductor tin oxide electrode, and making the free base porphyrin in direct contact with SnO₂ substrate in a $P_{Zn}-P-SnO_2$ arrangement.

The dependence of the photocurrent efficiency on the applied potential has been analyzed by other authors [52,78,79] and showed that recombination rates between photoinjected electrons and a dye cation increase as more negative potentials are applied to the semiconductor. Lower cell efficiencies at negative bias correlate with this increase in the charge recombination rate. These studies suggested that the increase in recombination rate constant at more negative potentials implies the level of the steady-state trap occupancy in the nanostructured semiconductor. In order to avoid this factor in the comparative analysis of the efficiency of the different dyes used in this work, the measurements were carried out under potential control. The effect of the applied potential on the observed photocurrent generation is shown in Fig. 8 for different ITO/SnO₂/dye electrodes. In this figure the value of the photocurrent quantum yield expressed as the $\Phi_{inj} \eta_c$ value of the systems at the Soret bands are plotted vs. the applied potential. $\Phi_{inj} \eta_c$ increases with the anodic bias in all cases, mainly due to the increase in the collection efficiency of the injected electrons.

Fig. 8 also shows that the photocurrent quantum yield is higher in the dyad molecule than for the separated moieties in all applied potential range. Moreover, the analysis of the photocurrent action spectra of the $P_{Zn}-P$ dyad in the 500–700 nm region shows that both porphyrin moieties contribute with similar quantum yield to the observed photoelectric effect. Fig. 9 shows the photocurrent and absorption spectra normalized to one at 520 nm, where only free base moiety absorbs radiation. The closely match between both spectra demonstrate that there is not difference in the contribution from the two moieties to the global photocurrent observed. Thus, the excitation of either moiety results in

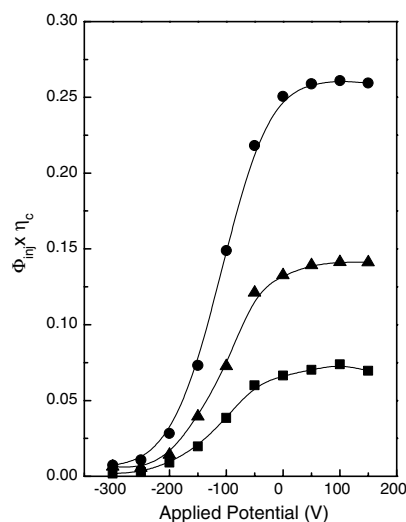


Fig. 8. Dependence of the product of the charge injection yield (Φ_{inj}) and charge collection efficiency η_c at the maximum of the Soret bands of ITO/SnO₂/P_{Zn}-P (●), ITO/SnO₂/P_{Zn} (▲) and ITO/SnO₂/P (■) electrodes on applied bias.

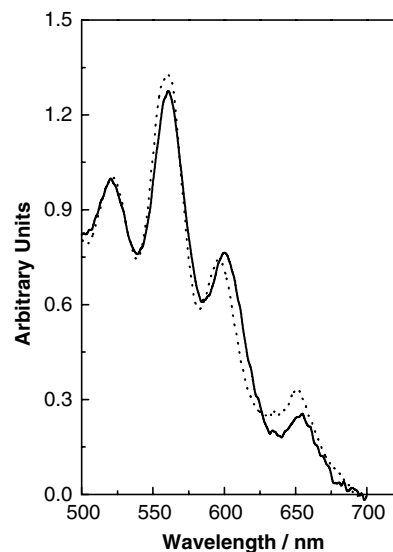


Fig. 9. Photocurrent (-----) and absorption (————) spectra of $P_{Zn}-P$ dyad in Q band wavelength region, normalized to one at 520 nm.

electron injection into SnO₂ conduction band, with similar electron harvesting capacity.

3.4. Laser-flash photolysis

The changes in the absorbance measured at 430 nm (dye's Soret band) following excitation after 3.0 mJ cm⁻² laser pulse at 532 nm for ITO/SnO₂/dye electrodes are shown in Fig. 10. Electron injection results in fast bleaching followed by regeneration of the ground state absorbance of the porphyrin compounds. As it has been reported for several dyes, including porphyrins

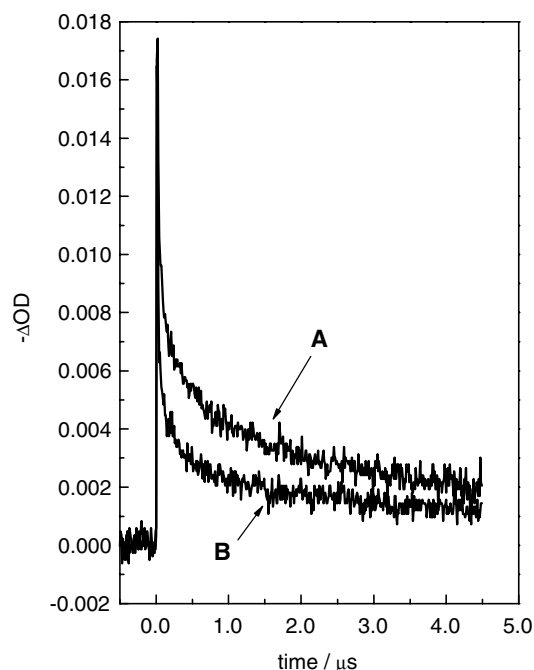


Fig. 10. Kinetic of dye neutral state recovery on SnO_2 followed at 430 nm after laser pulse for (a) $\text{ITO}/\text{SnO}_2/\text{P}$ and (b) $\text{ITO}/\text{SnO}_2/\text{P}_{\text{Zn}}-\text{P}$ electrodes, $\lambda_{\text{exc}} = 532$ nm, applied bias 0.05 V.

[53,80], the primary step of electron injection across the sensitizer/semiconductor interface is extremely fast in the case of TiO_2 semiconductor (<100 fs for tetracarboxyphenyl porphyrins [53]). In addition, Benkő et al. [81] demonstrated that the time constant and overall quantum yield of electron injection from RuN3 dye are similar for to both TiO_2 and SnO_2 semiconductors, the author concluded that electron injection process is almost independent of the semiconductor used.

The recovery processes, in absence of sacrificial donor hydroquinone, observed in Fig. 10 are associated with the reduction of the oxidized species formed after excitation and electron injection. The regeneration process, which occurs by recombination between photoinjected electron in the semiconductor and the oxidized dye, present a comparatively fast step followed by another slower one, showing a complex kinetics [82,83]. Such behavior is often observed in similar heterogeneous systems, and is attributed to multiple electrons trapping in surface defects, which affect the recovery process [84,85].

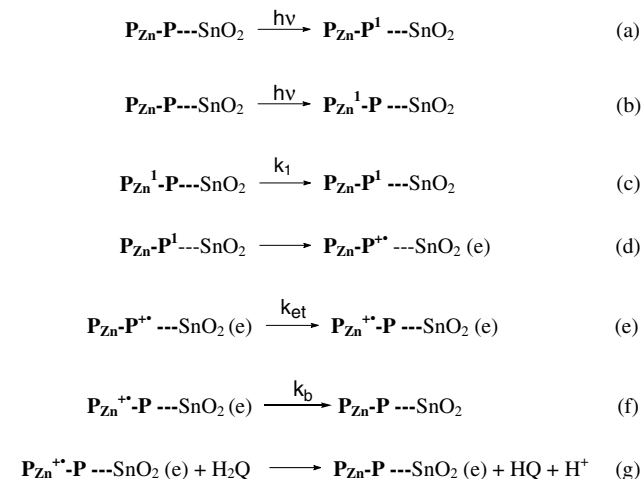
As can be observed in Table 1 (assuming pseudo first order kinetic constant denoted as k_b) back electron transfer is faster in the case of $\text{ITO}/\text{SnO}_2/\text{P}$ electrode than $\text{ITO}/\text{SnO}_2/\text{P}_{\text{Zn}}-\text{P}$. As was already mentioned, in despite of the fact that the electron injection efficiency is comparable for both compounds, **P** dye is less efficient in the generation of photoelectric effects than the dyad molecule. Thus, the charge collection efficiency of the systems, which is related to

electron percolation through the external circuit and recombination with the oxidized species, seems to be responsible of the observed different photocurrent quantum yield. Similar relationship between η_c and pseudo first order back electron transfer kinetic constant has been reported for a series of ruthenium (II) polypyridyl complexes [85].

However, it should be taking in account that in the kinetic analysis (Table 1) we assumed pseudo first order kinetic, fitted by a bi-exponential function. But it is known that the back electron transfer process is a very complex phenomenon which involves electrons occupying conduction band, superficial traps and bulk traps states [78,83], and consequently a quantitative analysis of the relation between k_b and $\Phi_{\text{inj}} \eta_c$ would be highly speculative. Moreover, has been reported that a proportion of charge recombination occurs on time scales less than the time resolution of our laser flash photolysis set-up [78]. On the other hand, as it has already been pointed out by Boschloo et al. [86], in practice rather high laser pulse intensities are needed in order to obtain sufficient signal in laser flash photolysis experiments on dye sensitized semiconductor electrodes, making a direct comparison with conditions that exit under normal illumination slight difficult.

In order to explain our results, a possible energy and electron transfer mechanism in the $\text{ITO}/\text{SnO}_2/\text{P}_{\text{Zn}}-\text{P}$ electrodes is given in the Scheme 1, according to the photophysical properties of $\text{P}_{\text{Zn}}-\text{P}$ dyad and the observed photoelectric effects.

According this Scheme, both porphyrins moieties in the dyad can be excited by light absorption (steps a and b), but the lack of fluorescence from the metallized unit (both in solution and in adsorbed state) indicates that energy transfer from $\text{P}_{\text{Zn}}^{\text{I}}$ state to **P** moiety occurs with high yield [51,54] (step c).



Scheme 1.

The heterogeneous electron transfer process able to generate photoelectric effect (step d) produces the formation of the radical cation $\mathbf{P}_{\text{Zn}}-\mathbf{P}^{+\bullet}$, but the intramolecular electron transfer from the \mathbf{P}_{Zn} to the oxidized free base (step e) is an exergonic process, as it is inferred from the 0.48 V difference in the oxidation potentials. As a consequence, regardless the electron injection pathway, it is proposed that the $\mathbf{P}_{\text{Zn}}^{+\bullet}-\mathbf{P}$ cation is formed (step e). Nonetheless, in a previous work we found that the presence of the oxidized \mathbf{P}_{Zn} enhanced the back electron transfer process in the case of a similar metallodiporphyrin [51]. This effect produces lower photocurrent yields in that dyad molecule in comparison with the corresponding monomers.

On the other hand, regardless of the fact that the compounds with higher back electron transfer rate constant have a corresponding lower photocurrent quantum yield (see Table 1), in agreement with the model that we suggested, \mathbf{P}_{Zn} and $\mathbf{P}_{\text{Zn}}-\mathbf{P}$ showed not so different recombination rates in the time scale of our laser flash photolysis experiment. As it was already mentioned, our kinetic analysis is an oversimplification of a complex one, and it is possible that more sophisticated experiments are needed (for example ultrafast transient absorption measurements) in order to obtain a more certain relationship between k_b and $\Phi_{\text{inj}} \eta_c$.

Nevertheless, in the present case, the photocurrent quantum yield is higher in the dyad molecule, when it is compared with the free base moiety. Since the dyad $\mathbf{P}_{\text{Zn}}-\mathbf{P}$ was designed with capacity for preferential orientation when it is adsorbed onto the semiconductor oxide (denoted in the Scheme 1 as $\mathbf{P}_{\text{Zn}}-\mathbf{P}-\text{SnO}_2$), the recombination process $\mathbf{P}_{\text{Zn}}^{+\bullet}-\mathbf{P}-\text{SnO}_2(e) \rightarrow \mathbf{P}_{\text{Zn}}-\mathbf{P}-\text{SnO}_2$ is shown to be less effective than when the oxidized sensitizer is in direct contact with the semiconductor, due to the exponential decay of the electron transfer rate constant with the distance. Consequently it is highly probable that the slower charge recombination kinetic in $\mathbf{P}_{\text{Zn}}-\mathbf{P}$ in comparison with \mathbf{P} is the responsible of the photocurrent yield observed in the dyad sensitized photoelectrodes.

4. Conclusions

A new porphyrin-porphyrin non-symmetric dyad has been used as light receptor in the spectral sensitization of nanocrystalline SnO_2 semiconductor electrode. The dyad contains structural moieties with both different singlet state energy and redox properties, and it is able to produce an electron transport – molecular antenna effect. The heterogeneous charge injection from $\mathbf{P}_{\text{Zn}}-\mathbf{P}$ is favored in the dyad due to the preferential orientation through the free carboxylic acid group of the \mathbf{P} moiety able to bind to the semiconductor surface. The close match between the photocurrent action spectrum and the absorption spectrum shows that the photosensitiza-

tion mechanism is operative in extending the photocurrent response of $\text{ITO}/\text{SnO}_2/\text{dye}$ electrode to the visible region. Also it demonstrates that the excitation of either moiety results in electron injection into SnO_2 conduction band, with similar electron harvesting capacity. It is proposed that inhibition of back electron transfer is favored by the slower charge recombination kinetic in the $\mathbf{P}_{\text{Zn}}^{+\bullet}-\mathbf{P}-\text{SnO}_2(e)$ state with respect to the case where the oxidized cation is in direct contact with the semiconductor. Moreover, fluorescence analysis of $\mathbf{P}_{\text{Zn}}-\mathbf{P}$ dyad and the \mathbf{P} moiety adsorbed on both SnO_2 and SiO_2 shows that the charge-injection yields (Φ_{inj}) from the excited dye to the tin oxide semiconductor in both cases are similar. Thus photocurrent enhancement is interpreted in terms of intramolecular electron transfer and preferential spatial orientation of the dyad on the SnO_2 surface that preclude back electron transfer. The architecture of dyad is a promising organic material for spectral sensitization of semiconductor solar cells.

Acknowledgements

We are grateful to Consejo Nacional de Investigaciones Científicas y Técnicas (CONICET-Argentina); Agencia Nacional de Promoción Científica y Tecnológica (ANPCYT-Argentina), Secretaría de Ciencia y Técnica de la Universidad Nacional de Río Cuarto (SECYT-UNRC) and Fundación Antorchas for financial support. L.O., E.N.D. and J.J.S. are scientific members of CONICET. M.E.M. and M.G. thank CONICET for a research fellowship. Thanks are also due to C.M. Previtali for his help in Laser Flash Photolysis experiments.

References

- [1] B. O'Regan, M. Grätzel, *Nature* 353 (1991) 737.
- [2] A. Kay, M. Grätzel, *Chem. Mater.* 14 (2002) 2930.
- [3] R.D. McConnell, *Renew. Sustainable Energy Rev.* 6 (2002) 271.
- [4] T. Stergiopoulos, I.M. Arabatzis, H. Cachet, P. Falaras, *J. Photochem. Photobiol. A: Chem.* 155 (2003) 163.
- [5] A. Kay, M. Grätzel, *J. Phys. Chem.* 97 (1993) 6272.
- [6] A. Kay, R. Humphry-Baker, M. Grätzel, *J. Phys. Chem.* 98 (1994) 952.
- [7] S. Hotchandani, P.V. Kamat, *Chem. Phys. Lett.* 191 (1992) 320.
- [8] I. Bedja, S. Hotchandani, R. Carpentier, R. Fessenden, P.V. Kamat, *J. Appl. Phys.* 75 (1994) 5444.
- [9] I. Bedja, P.V. Kamat, S. Hotchandani, *J. Appl. Phys.* 80 (1996) 4637.
- [10] H. Deng, H. Mao, Z. Lu, J. Li, H. Xu, *J. Photochem. Photobiol. A: Chem.* 110 (1997) 47.
- [11] G.K. Boschloo, A. Goossens, *J. Phys. Chem.* 100 (1996) 19489.
- [12] L. Otero, H. Osora, W. Li, M.A. Fox, *J. Porphyrins Phthalocyanines* 2 (1998) 123.
- [13] H.H. Deng, Z.H. Lu, *Supramol. Sci.* 5 (1998) 669.
- [14] J. Wienke, T.J. Schaafsma, A. Goossens, *J. Phys. Chem. B* 103 (1999) 2702.

- [15] M. Linke-Schaetzel, A.D. Bhise, H. Gliemann, T. Koch, T. Schimmel, T.S. Balaban, *Thin Solid Films* 451 (2004) 16.
- [16] G. Feher, J.P. Allen, M.I. Okamura, D.C. Rees, *Nature* 339 (1989) 111.
- [17] D. Gust, T. Moore, in: D. Volman, G. Hammond, D. Neckers (Eds.), *Advances in Photochemistry*, vol. 16, 1991, p. 1.
- [18] D. Kuciauskas, P.A. Liddell, S. Lin, T.E. Johnson, S.J. Weghorn, J.S. Lindsey, A.L. Moore, T.A. Moore, D. Gust, *J. Am. Chem. Soc.* 121 (1999) 8604.
- [19] M.R. Wasielewski, *Chem. Rev.* 92 (1992) 435.
- [20] S.L. Springs, D. Gosztola, M.R. Wasielewski, V. Král, A. Andrievsky, J.L. Sessler, *J. Am. Chem. Soc.* 121 (1999) 2281.
- [21] H. Imahori, D.M. Guldi, K. Tamaki, Y. Yoshida, C. Luo, Y. Sakata, S. Fukuzumi, *J. Am. Chem. Soc.* 123 (2001) 6617.
- [22] H. Imahori, K. Tamaki, Y. Araki, T. Hasobe, O. Ito, A. Shimomura, S. Kundu, T. Okada, Y. Sakata, S. Fukuzumi, *J. Phys. Chem. A* 106 (2002) 2803.
- [23] H. Imahori, Y. Mori, Y. Matano, *J. Photochem. Photobiol. C: Photochem. Rev.* 4 (2003) 51.
- [24] A.F. Noriega, L.F.O. Frutado, A.L.B. Formiga, M. Nakamura, K. Araki, H.E. Toma, *Inorgan. Chem.* 43 (2004) 396.
- [25] J.N. Clifford, E. Palomares, M.K. Nazeeruddin, R. Thampi, M. Gratzel, J.R. Durrant, *J. Am. Chem. Soc.* 126 (2004) 5670.
- [26] H. Deng, Z. Lu, Y. Shen, H. Mao, H. Xu, *Chem. Phys.* 231 (1998) 95.
- [27] K. Takahashi, I. Nakajima, K. Imoto, T. Yamaguchia, T. Komura, K. Murata, *Sol. Energy Mater. Sol. Cells* 76 (2003) 115.
- [28] J. Chen, A.K. Burrell, W.M. Campbell, D.L. Officer, C.O. Too, G.G. Wallace, *Electrochim. Acta* 49 (2004) 329.
- [29] K. Miyairi, E. Itoh, Y. Hashimoto, *Thin Solid Films* 438 (2003) 147.
- [30] J.H. Yu, F. Li, X. Wang, Y. Huang, B. Zhang, C. Huang, Y. Cao, *Opt. Mater.* 21 (2003) 467.
- [31] D. Wróbel, J. Lukaszewicz, J. Goc, A. Waszkowiak, R. Ion, *J. Mol. Struct.* 555 (2000) 407.
- [32] D. Wróbel, *Comptes Rendus Chimie* 6 (2003) 417.
- [33] J.E. Moser, P. Bonhôte, L. Walder, M. Grätzel, *Chimia* 51 (1997) 28.
- [34] M.K. Nazeeruddin, A. Kay, I. Rodicio, R. Humphry-Baker, E. Muller, P. Liska, N. Vlachopoulos, M. Grätzel, *J. Am. Chem. Soc.* 115 (1993) 6382.
- [35] G. Smestad, *Sol. Energy Mater. Sol. Cells* 32 (1994) 273.
- [36] A. Hagfeld, M. Grätzel, *Chem. Rev.* 95 (1995) 49.
- [37] P.V. Kamat, *Prog. React. Kinetics* 19 (1994) 277.
- [38] I. Bedja, S. Hotchandani, P.V. Kamat, *J. Phys. Chem.* 98 (1994) 4133.
- [39] P.V. Kamat, *CHEMTECH* 25 (1995) 22.
- [40] P.V. Kamat, I. Bedja, S. Hotchandani, L. Patterson, *J. Phys. Chem.* 100 (1996) 4900.
- [41] I. Bedja, P.V. Kamat, X. Hua, A.G. Lappin, S. Hotchandani, *Lagmuir* 13 (1997) 2398.
- [42] H. Sugihara, L.P. Singh, K. Sayama, H. Arakawa, M.K. Nazeeruddin, M. Grätzel, *Chem. Lett.* 10 (1998) 1005.
- [43] S.D. Burnside, K. Brooks, A.J. McEvoy, M. Grätzel, *Chimia* 52 (1998) 557.
- [44] H. Imahori, H. Yamada, Y. Nishimura, I. Yamazaki, Y. Sakata, *J. Phys. Chem. B* 104 (2000) 2099.
- [45] H. Imahori, H. Norieda, H. Yamada, Y. Nishimura, I. Yamazaki, Y. Sakata, S. Fukuzumi, *J. Am. Chem. Soc.* 123 (2001) 100.
- [46] D. Hirayama, K. Takimiya, Y. Aso, T. Otsubo, T. Hasobe, H. Yamada, H. Imahori, S. Fukuzumi, Y. Sakata, *J. Am. Chem. Soc.* 124 (2002) 532.
- [47] T. Hasobe, H. Imahori, S. Fukuzumi, P.V. Kamat, *J. Phys. Chem. B* 107 (2003) 12105.
- [48] T. Hasobe, H. Imahori, P.V. Kamat, S. Fukuzumi, *J. Am. Chem. Soc.* 125 (2003) 14962.
- [49] F. Fungo, L. Otero, C.D. Borsarelli, E.N. Durantini, J.J. Silber, L. Sereno, *J. Phys. Chem. B* 106 (2002) 4070.
- [50] F. Fungo, L. Otero, L. Sereno, J.J. Silber, E.N. Durantini, *J. Mater. Chem.* 10 (2000) 645.
- [51] F. Fungo, L. Otero, E.N. Durantini, J.J. Silber, L. Sereno, *J. Phys. Chem. B* 104 (2000) 7644.
- [52] S.A. Haque, Y. Tachibana, D.R. Klug, J.R. Durrant, *J. Phys. Chem. B* 102 (1998) 1745.
- [53] Y. Tachibana, S.A. Haque, I.P. Mercer, J.R. Durrant, D.R. Klug, *J. Phys. Chem. B* 104 (2000) 1198.
- [54] R.B.M. Koehorst, G.K. Boschloo, T.J. Savenije, A. Goossens, T.J. Schaafsma, *J. Phys. Chem. B* 104 (2000) 2371.
- [55] M.A. Milanesio, M. Gervaldo, L. Otero, L. Sereno, J.J. Silber, E.N. Durantini, *J. Porphyrins Phthalocyanines* 7 (2003) 42.
- [56] K.M. Kadish, M.M. Morrison, *J. Am. Chem. Soc.* 98 (1976) 3326.
- [57] K.M. Kadish, M.M. Morrison, *Inorg. Chem.* 15 (1976) 980.
- [58] K.M. Kadish, M.M. Morrison, *Bioinorg. Chem.* 7 (1977) 107.
- [59] F.A. Walker, D. Beroiz, K.M. Kadish, *J. Am. Chem. Soc.* 98 (1976) 3484.
- [60] D. Gust, T.A. Moore, A.L. Moore, L. Leggett, S. Lin, J.M. DeGraziano, R.M. Hermant, D. Nicodem, P. Craig, G.R. Seely, R.A. Nieman, *J. Phys. Chem.* 97 (1993) 7926.
- [61] D. Gust, T.A. Moore, A.L. Moore, H.K. Kang, J.M. DeGraziano, P.A. Liddell, G.R. Seele, *J. Phys. Chem.* 97 (1993) 13637.
- [62] T. Ma, K. Inoue, K. Yao, H. Noma, T. Shuji, E. Abe, J. Yu, X. Wang, B. Zhang, *J. Electroanal. Chem.* 537 (2002) 31.
- [63] T. Ma, K. Inoue, H. Noma, K. Yao, E. Abe, *J. Photochem. Photobiol. A: Chem.* 152 (2002) 207.
- [64] P. Bonhôte, J.-E. Moser, R. Humphry-Baker, N. Vlachopoulos, S.M. Zakeeruddin, L. Walder, M. Grätzel, *J. Am. Chem. Soc.* 121 (1999) 1324.
- [65] J.N. Clifford, E. Palomares, M.K. Nazeeruddin, M. Gratzel, J. Nelson, X. Li, N.J. Long, J.R. Durrant, *J. Am. Chem. Soc.* 126 (2004) 5225.
- [66] G.R. Geier III, J.S. Lindsey, *J. Chem. Soc. Perkins Trans. 2* (2001) 677.
- [67] E.N. Durantini, J.J. Silber, *Synth. Commun.* 29 (1999) 3353.
- [68] T. Stergiopoulos, I.M. Arabatzis, H. Cachet, P. Falaras, *J. Photochem. Photobiol. A: Chem.* 155 (2003) 163.
- [69] N.-G. Park, M.G. Kang, K.S. Ryu, K.M. Kim, S.H. Chang, *J. Photochem. Photobiol. A: Chem.* 161 (2004) 105.
- [70] H. Gerischer, F. Willig, *Top. Curr. Chem.* 61 (1976) 31.
- [71] C.D. Borsarelli, J.J. Cosa, C.M. Previtali, *Photochem. Photobiol.* 68 (1998) 438.
- [72] K.M. Kadish, N. Guo, E. Van Caemelbeckie, R. Paolesse, D. Monti, P. Tagliatesta, *J. Porphyrins Phthalocyanines* 2 (1998) 439.
- [73] D. Gust, T. Moore, A. Moore, F. Gao, D. Luttrull, J. DeGraziano, X. Ma, L. Makings, S.-J. Lee, T. Trier, E. Bittersmann, G. Seely, S. Woodward, R. Bensansson, M. Rougée, F. De Schryver, M. Van der Auweraer, *J. Am. Chem. Soc.* 113 (1991) 3638.
- [74] T. Kajiwara, K. Hashimoto, T. Kawal, T. Sakata, *J. Phys. Chem.* 86 (1982) 4516.
- [75] T. Sakata, K. Hashimoto, M. Hiramoto, *J. Phys. Chem.* 94 (1990) 3040.
- [76] K. Hashimoto, M. Hiramoto, T. Sakata, *J. Phys. Chem.* 92 (1988) 4272.
- [77] P. Vlachopoulos, P. Liska, J. Augustynski, M. Grätzel, *J. Am. Chem. Soc.* 110 (1988) 1216.
- [78] S.A. Haque, Y. Tachibana, R.L. Willis, J.E. Moser, M. Gratzel, D.R. Klug, J.R. Durrant, *J. Phys. Chem. B* 104 (2000) 538.
- [79] D. Kuciauskas, M.S. Freund, H.B. Gray, J.R. Winkler, N.S. Lewis, *J. Phys. Chem. B* 105 (2001) 392.
- [80] Y. Tachibana, M.K. Nazeeruddin, M. Gratzel, D.R. Klug, J.R. Durrant, *Chem. Phys.* 285 (2002) 127.

- [81] G. Benkő, P. Myllyperkiö, J. Pan, A.P. Yartsev, V. Sundström, J. Am. Chem. Soc. 125 (2003) 1118.
- [82] J. Bisquert, A. Zaban, P. Salvador, J. Phys. Chem. B 106 (2002) 8774.
- [83] J. Bisquert, A. Zaban, M. Greenshtein, I. Mora-Sero, I.J. Am. Chem. Soc. 126 (2004) 13550.
- [84] C. Graziani Garcia, C.J. Kleverlaan, C.A. Bigozzi, N.Y.M. Iha, J. Photochem. Photobiol. A: Chem. 147 (2002) 143.
- [85] C. Graziani Garcia, A.K. Nakano, C.J. Kleverlaan, N.Y.M. Iha, J. Photochem. Photobiol. A: Chem. 151 (2002) 165.
- [86] G. Boschloo, A. Hagfeldt, Chem. Phys. Lett. 370 (2003) 381.